ACS APPLIED MATERIALS & INTERFACES

www.acsami.org

Research Article

All-Natural, Robust, and pH-Responsive Glycyrrhizic Acid-Based Double Network Hydrogels for Controlled Nutrient Release

Qing Li, Xinke Yu, Shiqi Zhang, Mengyue Xu, Yunyi Yang, Zhili Wan,* and Xiaoquan Yang

Cite This: *ACS Appl. Mater. Interfaces* 2023, 15, 43633−43647

Read Online

ACCESS | Metrics & More | Article Recommendations | Supporting Information

ABSTRACT: Supramolecular hydrogels self-assembled from naturally occurring small molecules (e.g., glycyrrhizic acid, GA) are promising materials for controlled bioactive delivery due to their facile fabrication processes, excellent biocompatibility, and versatile stimuli-responsive behaviors. However, most of these natural hydrogels suffer from poor mechanical strength and processability for practical applications. In this work, through adopting a multicomponent gel approach, we developed a novel mechanically robust GA-based hydrogel with an interpenetrating double network (DN) that is composed of a Ca^{2+}-enhanced hydrogen-bond supramolecular GA nanofibril (GN) network and a Ca^{2+}cross-linked natural polysaccharide sodium alginate (ALG) network. Compared to the single GN network (SN) hydrogel, the GN-ALG hybrid hydrogels (GN-ALG-DN) with the hierarchical double-network structure possess excellent mechanical properties and shaping adaptation, encouraging small and large amplitude oscillatory shear (SAOS and LAOS) rheological performances, better thermal stability, higher resistance to large compression deformations, and lower swelling behaviors. Furthermore, the GN-ALG-DN hydrogels exhibit a pH-responsive and sustained release behavior of nutrients (i.e., vitamin B_{12}, VB_{12}), showing a faster VB_{12} release rate with a higher swelling ratio in an alkaline condition (pH 7.5) than in an acidic condition (pH 2.5). This is ascribed to the fact that the higher dissociation degree of carboxylic groups in GA and ALG molecules in an alkaline environment induces the erosion and looseness of the self-assembled GN network and the ionic-cross-linked ALG network, which can lead to the decomposition of the hybrid hydrogels and thereby increases the release of nutrients. Cytotoxicity tests further demonstrate the excellent biocompatibility of the GN-ALG-DN hydrogels. This study highlights the design of robust shaped and structured supramolecular hydrogels from natural herb small molecules, which can serve as solid, edible, and stimuli-responsive active cargo delivery platforms for food, biomedical, and sustainable applications.

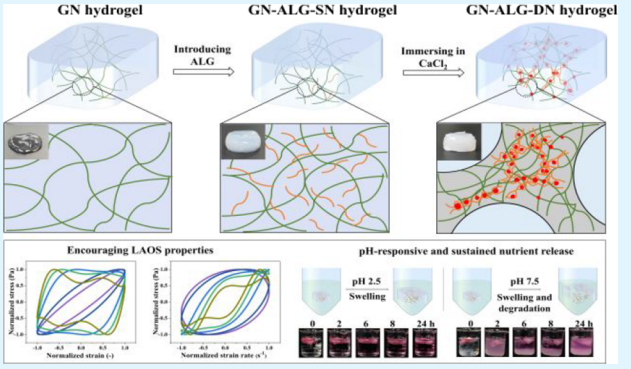

KEYWORDS: *glycyrrhizic acid, hydrogels, Ca^{2+}-cross-linked alginate network, pH-responsive release, biocompatibility*

1. INTRODUCTION

Supramolecular hydrogels are fascinating and versatile functional soft materials that are generally formed from the self-assembly of small molecules (i.e., low-molecular-weight gelators, LMWGs) through noncovalent interactions.[1−5] The LMWG hydrogels, especially those obtained from naturally occurring small molecules or their derivatives, have been increasingly explored for promising applications in various biological fields including drug delivery, wound healing, tissue regeneration, and biosensors, due to their facile fabrication processes, excellent biocompatibility and biodegradability, and multiresponsive behaviors to external stimuli (e.g., temperature, pH, and ionic strength).[6−11] However, these natural LMWG hydrogels with weak noncovalent cross-linked networks usually have poor mechanical strength and limited ability to be shaped and can be easily destroyed during processing, which severely limits the breadth of their practical applications.[12,13] Various strategies, including double-network (DN) hydrogels, nanocomposite hydrogels, and microgel-reinforced hydrogels, have been attempted to shape and structure LMWG hydrogels for achieving the ideal material properties.[14−16] Among them, developing hybrid hydrogels with a DN structure by combining the self-assembled LMWG network and a mechanically strong polymer gel network, leading to a self-sorting multicomponent hydrogel, has been demonstrated to be an effective and potentially powerful approach to shaping and structuring LMWG-based supramolecular gels.[12,17−20] The obtained DN hydrogels can combine the advantages of both networks, including the

Received: July 19, 2023
Accepted: August 29, 2023
Published: September 11, 2023

https://doi.org/10.1021/acsami.3c10407
ACS Appl. Mater. Interfaces 2023, 15, 43633−43647

responsive, tunable, and programmable nature of the LMWG network and the high mechanical strength of the polymer gel network, as well as their mutual interactions, which can endow the hybrid hydrogels with advanced materials performance for use in a variety of applications.

Glycyrrhizic acid (GA) is a natural saponin derived from the root of the licorice plant, which possesses various biological activities including anti-inflammation, hepatoprotective, anticancer, and antiviral activities.[21−24] GA is a polyprotic weak acid with three carboxylic groups, and thus it has three dissociation constant pK_a values (3.98, 4.62, and 5.17). GA molecule has a typical amphiphilic structure, which is composed of a hydrophobic triterpenoid aglycone moiety (18β-glycyrrhetinic acid) bound at position C-3 via an ether bond to a hydrophilic diglucuronic unit. Owing to the structural amphiphilicity and chirality, GA molecules display anisotropic self-assembly behavior in water, leading to the formation of semiflexible GA nanofibrils (GN), which can further form supramolecular hydrogels with a hydrogen-bond three-dimensional fibrillar network.[25,26] Moreover, the multiple functional groups, rigid skeletons, and unique stacking behaviors of GA molecules render them suitable as an ideal platform for creating various GA derivatives, which can be further used for constructing versatile hydrogel materials.[27,28] We recently found that the self-assembled GN also have favorable interfacial activity, displaying a multidimensional assembly at liquid interfaces (i.e., oil−water and air−water interfaces) and in the aqueous phase, which makes them highly suitable as edible stabilizers for producing multiphase soft materials with high stability, stimulability, and processability.[26,29−32] In view of the unique combination of directed self-assembly and inherent strong biological activity, the natural GA and self-assembled GN can be used as ideal bifunctional building blocks for fabricating bioactive supramolecular herb hydrogels, which are expected to have wide applications in functional food and biomedical fields. However, as a typical LMWG hydrogel, the GA supramolecular hydrogels also suffer from poor mechanical strength and processability due to their weak noncovalent network linkages, which thus largely limit their practical use. Recently, to address these limitations of GA hydrogels, we developed an interpenetrating dual-network hydrogel by first adopting a mild oxidation strategy to obtain an aldehyde-contained GA hydrogen-bond fibrillar network, followed by complexation with a biopolymer carboxymethyl chitosan,[33] forming a secondary Schiff base covalent network. The prepared GA-based hydrogels exhibit adequate mechanical strength and multiple functions, including injectability, shape adaptation and remodeling, self-healability, and favorable adhesiveness, which can serve as an efficient dressing material to promote wound healing. However, the aldehyde-grafted GA molecules are chemically modified substances that, to some extent, can impair the biocompatibility of natural GA and raise the safety concerns of the hydrogels.

Considering the great potential of GA-based bioactive herb hydrogels as promising biomaterials, it is highly desirable to explore new and sustainable strategies for developing novel mechanically robust GA-based hydrogels with remarkable multifunctional properties, including excellent shaping ability, high thermostability, and swelling resistance. Herein, based on the aforementioned strategies for improving the materials properties of LMWG hydrogels, we attempt to employ a multicomponent approach to endow the GA supramolecular hydrogels with sufficient mechanical strength and multifunctionality without any chemical modification of the GA molecules, which is achieved through the incorporation of a mechanically strong polymer gel network into the self-assembled GN network, creating the hybrid hydrogels with a hierarchical DN structure. To achieve this robust DN hydrogel, we first choose a natural polysaccharide sodium alginate (ALG), which is a fascinating food-grade biopolymer gelator with excellent availability, biocompatibility, biodegradability, and can form strong hydrogels in the presence of multivalent cations (e.g., Ca^{2+}) by generating an ionic cross-linking network.[34,35] After the incorporation of ALG solution into the GN fibrillar network (GN-ALG), the GN-ALG DN hydrogels can be created by diffusing a $CaCl_2$ solution into the formed first GN-ALG network matrix, in which the Ca^{2+} not only induces the generation of the new ALG network but also can enhance the GN fibrillar network, leading to the formation of a unique interpenetrating DN that comprises the Ca^{2+}-enhanced self-assembled hydrogen-bond GN network and the Ca^{2+}-cross-linked ALG gel network. As a self-sorting multicomponent gel system, the resulting GN-ALG hybrid hydrogels with DN structure possess adequate mechanical strength and multifunctional properties, including high shaping ability, excellent rheological and thixotropy recovery properties, high large deformation resistance performance, and low swelling properties. Moreover, these robust hybrid hydrogels with excellent biocompatibility exhibit an interesting pH-responsive behavior, which enables them to have the capacity to be an ideal delivery vehicle for the controlled release of bioactives and nutrients. Therefore, through the multicomponent gel approach, this work demonstrates the facile and efficient development of robust and multifunctional supramolecular hydrogels from natural herb small molecules. Compared with the hydrogels made of synthetic and even potentially toxic LMWGs, these all-natural, edible GA-based hydrogels with remarkable characteristics and properties can have more sustainable applications in those requiring high biosafety, such as functional foods and controlled delivery and release for biomedical use.

2. MATERIALS AND METHODS

2.1. Materials. Glycyrrhizic acid mono ammonium salt (GA, purity >98%, molecular weight: 839.98 g/mol) was purchased from Acros Organics (USA). Sodium alginate (ALG, molecular weight: 120,000 g/mol), vitamin B_{12} (VB_{12}), and calcium chloride anhydrous ($CaCl_2$) were purchased from Aladdin (Shanghai, China). TrypLE Express Enzyme, 1 × penicillin-streptomycin-glutamine, house serum, and Dulbecco's phosphate-buffered saline (DPBS) were purchased from Thermo Fisher Scientific. Methyl-thiazolyl diphenyl-tetrazolium bromide (MTT), dimethyl sulfoxide (DMSO), and minimum essential medium Eagle (MEM) were purchased from Sigma-Aldrich. Other chemicals were of analytical grade. All solutions were prepared using Milli-Q ultrapure water (18.2 MΩ·cm at 25 °C).

2.2. Fabrication of GN/ALG Single-Network Hydrogels. GN stock solution (2%, w/v) was obtained by dissolving GA powders in water at 80 °C until complete dissolution. ALG stock solution (2%, w/v) was prepared by dissolving ALG powder in water at room temperature (25 °C) for 1 h, and then, the pH was adjusted to 4.5. Pure GN hydrogel (GN) was obtained by first diluting GN stock solution at 80 °C to 1%, followed by cooling at 25 °C. The Ca^{2+}-enhanced GN single-network hydrogels (GN-SN) were fabricated by immersing the GN hydrogel into a $CaCl_2$ solution (5%, v/v) for 1 h. The ALG single-network hydrogels (ALG-SN) were prepared by adding a $CaCl_2$ solution (5%, v/v) into the ALG solution (1%, pH 4.5) for 1 h of cross-linking. The ALG-incorporated GN single-network hydrogels (GN-ALG-SN) were prepared by mixing ALG and

https://doi.org/10.1021/acsami.3c10407
ACS Appl. Mater. Interfaces 2023, 15, 43633−43647

GN solutions at 80 °C for 10 min, which were then left undisturbed at 25 °C to trigger gel formation. For these GN-ALG-SN hydrogels, the final concentration of GN is 1%, and the ALG concentration ranges from 0.2 to 1%, which were named GN-ALG$_{0.2}$-SN, GN-ALG$_{0.4}$-SN, GN-ALG$_{0.6}$-SN, GN-ALG$_{0.8}$-SN, and GN-ALG$_1$-SN, respectively.

2.3. Fabrication of GN-ALG Double-Network Hydrogels. GN-ALG double-network hydrogels (GN-ALG-DN) were obtained by immersing preprepared GN-ALG-SN hydrogels into the $CaCl_2$ solution (0.5−5%, v/v) for 1 h, which were then washed with water several times to remove the excess Ca^{2+}. The final concentration of GN is 1%, and the ALG concentration ranges from 0.2 to 1%. The corresponding hydrogels were named GN-ALG$_{0.2}$-DN, GN-ALG$_{0.4}$-DN, GN-ALG$_{0.6}$-DN, GN-ALG$_{0.8}$-DN, and GN-ALG$_1$-DN, respectively. The preparation of the VB$_{12}$-loaded DN hydrogel, GN-ALG-DN (VB$_{12}$), was performed by the same procedure by adding VB$_{12}$ (1 mg/mL) to the GN stock solution prior to gel formation.

2.4. Characterization. *2.4.1. Fourier Transform Infrared (FTIR) Spectroscopy.* Freeze-dried hydrogels were scanned from 4000 to 400 cm^{-1} with a resolution of 2 cm^{-1}. FTIR measurements were carried out on a Bruker Vertex 70 FTIR spectrometer.

2.4.2. Field-Emission Scanning Electron Microscopy (FE-SEM). The microstructure of freeze-dried hydrogels was examined by using a Zeiss Merlin field emission scanning electron microscope. The samples were sputtered with a thin layer of gold (JEOL JFC-1200 fine coater) before imaging.

2.4.3. Linear Small Amplitude Oscillatory Shear (SAOS) Rheology. The small amplitude oscillatory rheological measurements of hydrogels were performed on a HAAKE MARS 60 rheometer (HAAKE Co., Germany) equipped with a universal Peltier system and a water bath (HAAKE A40) for temperature control. A plate−plate geometry (35 mm diameter and 2.0 mm gap) was used for all measurements. Before the tests, samples were allowed to relax for 2 min. The oscillatory shear tests, including strain amplitude sweeps (0.01−1000%, frequency = 1 Hz) and frequency sweeps (0.1−100 Hz, strain = 0.1%, within the linear viscoelastic region, LVR), were performed at room temperature (25 °C). The damping factors (G''/G') of hydrogels at a constant frequency of 1 Hz and a fixed stress (1 Pa) were collected from the frequency sweeps. The frequency dependence of G' and G'' was analyzed using a power-law model, where the coefficients K′ and K″ are power-law constants (Pa·s^n), and n' and n'' are the frequency exponents (dimensionless):

$$G' = K' \cdot \omega^{n'} \tag{1}$$

$$G'' = K'' \cdot \omega^{n''} \tag{2}$$

The viscosity of the hydrogels was also analyzed at different shear rates (0.01−100 s^{-1}). The thixotropic behavior of hydrogels was then carried out at 25 °C by measuring the G' data with time at alternating low stress (10 Pa, within LVR) and high stress (1000 Pa, beyond LVR). Temperature sweeps were obtained by heating samples from 25 to 120 °C at a rate of 2 °C/min, at a constant strain of 0.1%, and at a frequency of 1 Hz.

2.4.4. Nonlinear Large Amplitude Oscillatory Shear (LAOS) Rheology. The torque-deformation waveform data at different strains (0.5, 1, 5, 10, and 50%) and a fixed frequency (1 Hz) were first collected using a HAAKE MARS60 rheometer (HAAKE Co., Germany) with native rheometer control software (Rheowin Job Manager). Then, the torque-deformation waveform data were further analyzed using the MITLaos software (ver. 2.2 beta). The raw strain−stress data were collected at a sampling rate of 512 s^{-1}. The signal-to-noise ratio (S/N) is the ratio of the amplitude of the highest peak (the first harmonic) divided by the standard deviation of the noise. Based on the resulting Fourier spectrum, the ratio of S/N (10^3−10^5) was estimated at the strains of 0.5, 1, 5, 10, and 50%, for all samples in this study.

S and T factors were used as indicators of intracycle behaviors, which were defined by the following equations:

$$S = \frac{G'_L - G'_M}{G'_L} \tag{3}$$

$$T = \frac{\eta'_L - \eta'_M}{\eta'_L} \tag{4}$$

where G'_M is the shear elastic modulus at minimum deformation (the slope of strain−stress Lissajous plot at zero strain), and G'_L means the shear elastic modulus at maximum deformation. The viscosity parameters η'_L and η'_M mean the viscosity at the maximum or minimum shear rate, respectively. Note that $S = 0$ is for a single harmonic linear elastic response. The values of the S factor above and below zero mean the behavior of samples is intracycle strain stiffening and strain softening, respectively. Similarly, $T = 0$ means a linear viscous response, $T > 0$ corresponds to intracycle shear thickening, and $T < 0$ represents intracycle shear thinning.

2.4.5. Large Deformation Compression. The large deformation compression test of hydrogels was performed using a universal testing machine (Instron 5943, USA). A cylindrical probe of 25 mm was used to compress cube hydrogels to a depth of 90% of their original height at a rate of 10 mm/s with a 0.1 N trigger value. The displacement distance was calculated relative to the starting point for each sample and reported as the relative displacement. The compression strain and stress were recorded during the tests. Fracture strain, fracture stress, and Young's modulus (i.e., elastic modulus, the slope of the linear part of a stress−strain curve at relatively small deformation) are calculated based on the stress−strain curves. For the loading−unloading test, the compression depth is fixed at 50% of the original height of the cube hydrogels. All of the tests were performed at 25 °C and samples were tested at least 3 times.

2.4.6. Swelling Properties. The swelling properties of the hydrogels were characterized by the swelling ratio. The freeze-dried hydrogels were weighed and then immersed in water and PBS solutions (0.05 M) with different pH values (2.5, 4.5, and 7.5) for swelling at different times. The swelling ratio was calculated by the following equation:

$$\text{Swelling ratio (\%)} = \frac{W_t - W_i}{W_i} \times 100 \tag{5}$$

where W_i and W_t are the weight of the initially dried hydrogels and the swollen hydrogels at different times, respectively.

2.5. Controlled Cargo Release. To investigate the bioactive release behavior of hydrogels under different pH conditions, we selected VB$_{12}$ as a model hydrophilic cargo to prepare functional hydrogels. VB$_{12}$ (1 mg/mL) was added to the GN stock solution before the incorporation of the ALG solution. Appropriate amounts of VB$_{12}$-loaded wet hydrogels and dried hydrogels were weighed into glass vials, followed by adding PBS solutions (0.05 M) at different pH values and then incubating under mild stirring (100 rpm) at 25 °C. The released solution was periodically removed, and the absorbance of the released VB$_{12}$ was measured at 361 nm using a UV−vis spectrophotometer (C40 Touch, Implen, Germany). VB$_{12}$ concentration was calculated according to a previously performed calibration curve. Meanwhile, equal volumes of the corresponding PBS solution were placed in the glass vials to maintain a constant volume. The release ratio of VB$_{12}$ was calculated according to the equation below:

$$\text{Release ratio (\%)} = \frac{C_t - C_0}{C_0} \times 100 \tag{6}$$

where C_0 and C_t mean the initial B_{12} concentration and B_{12} concentration at time t, respectively.

2.6. Cytocompatibility. The mouse fibroblast cells (L929) were used to evaluate the cytocompatibility of the GN-ALG-DN hydrogels. The complete medium consisted of modified Eagle medium (MEM, GIBCO), 10% fetal bovine serum (FBS, GIBCO), and 1% penicillin/streptomycin (GIBCO). The biocompatibility of hydrogels was determined by using the material extract protocol and MTT reduction assays. Hydrogel extract liquid was obtained by adding 200 mg of hydrogels to 10 mL of MEM media and incubating in an incubator (37 °C, 5% CO_2) for 24 h. Then, extracted liquids were diluted with MEM media at different ratios (1:1, 1:5, and 1:25). The L929 cells were first harvested in complete media in an atmosphere of 5% CO_2 at 37 °C for 24 h and then seeded in 96-well microtiter plates at a

https://doi.org/10.1021/acsami.3c10407
ACS Appl. Mater. Interfaces 2023, 15, 43633−43647

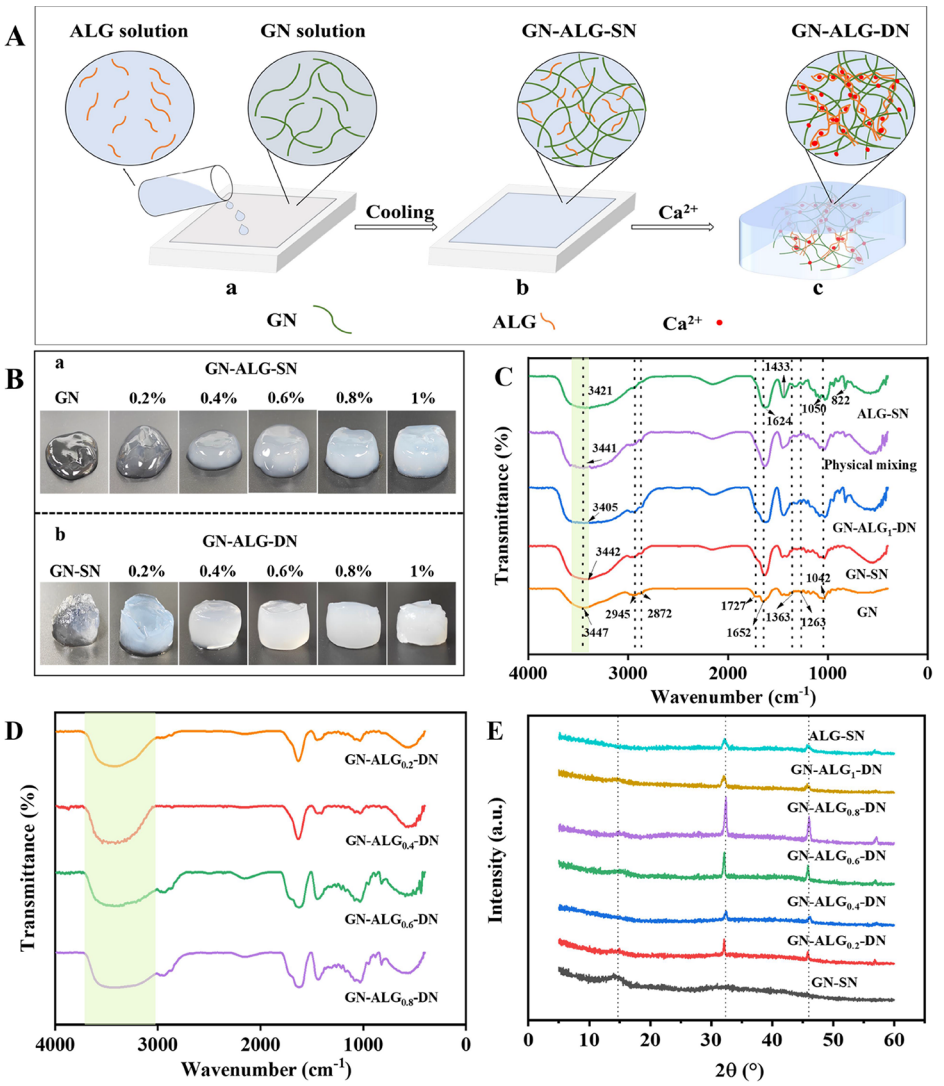

Figure 1. (A) Schematic diagram of the fabrication process for GN-ALG-DN hydrogels. (a) Mixing the ALG and GN solutions (pH 4.5) at 80 °C; (b) GN-ALG-SN hydrogels with a single GN fibrillar network, obtained by cooling the mixed solution at room temperature (25 °C); (c) GN-ALG-DN hydrogels with an interpenetrating double network, formed by immersing the above GN-ALG-SN hydrogels in $CaCl_2$ solution. (B) Photographs of (a) GN-ALG-SN hydrogels with 1% GN and different ALG concentrations (0−1%), and (b) the corresponding GN-ALG-DN hydrogels after immersion in 5% $CaCl_2$ solution. (C) FTIR spectra of GN hydrogel without Ca^{2+} (GN), Ca^{2+}-enhanced GN hydrogel (GN-SN), Ca^{2+}-cross-linked ALG hydrogel (ALG-SN), and GN-ALG-DN hydrogel at the same GN (1%) and ALG (1%) concentration (GN-ALG_1-DN). The mixture of dried GN and ALG hydrogel powders (physical mixing) was used as a control sample. (D) FTIR spectra of GN-ALG-DN hydrogels with 1% GN and different ALG concentrations (0.2−0.8%). (E) XRD spectra of these hydrogels.

density of 1×10^4 cells/well. After incubation for 24 h, the media were replaced with fresh media containing the hydrogel extract liquids with different diluted ratios. Following incubation of the cells with varying concentrations of hydrogel extract liquids for 24 h, the media were replaced by fresh MTT solution (0.5 mg/mL) and cultured with 5% CO_2 for 4 h at 37 °C, which was then used for the measurements of absorbance at 570 nm using a microplate reader. The untreated cells were set as a control. Live/dead staining was performed to further assess the cell cytotoxicity after being cultured with hydrogel-diluted liquids (20 mg/mL) for 24 h, where the live cells were stained by Calcein-AM with green fluorescence, and dead cells were stained by propidium iodide (PI) with red fluorescence. Five replicate wells were used for each sample, and all tests were repeated three times.

2.7. Statistical Analysis. Unless specified in our experiments, at least three freshly prepared samples were characterized. Mean values and standard deviations were determined for all measurements by using an analysis of variance (ANOVA) procedure from the SPSS 21.0 statistical analysis program. Duncan's test was used to compare mean values among three treatments, utilizing a level of significance of 5%.

3. RESULTS AND DISCUSSION

3.1. Fabrication of GN-ALG-DN Hydrogels. The self-assembly property of GN makes them suitable as building blocks to create supramolecular hydrogels with 3D fibrillar networks.[25,26] However, pure GN hydrogels suffer from poor mechanical strength and processability, which largely limit their practical applications in food and biomedical fields. Herein, through adopting a multicomponent gel approach, we fabricated a GN-based DN hydrogel with strong mechanical performance and remarkable multifunctional properties including excellent shaping ability, high thermostability, low swelling property, and pH-responsive and sustained release behavior of nutrients. ALG solution was first incorporated into the GN fibrillar network (SN) to create a series of GN-ALG

https://doi.org/10.1021/acsami.3c10407
ACS Appl. Mater. Interfaces 2023, 15, 43633−43647

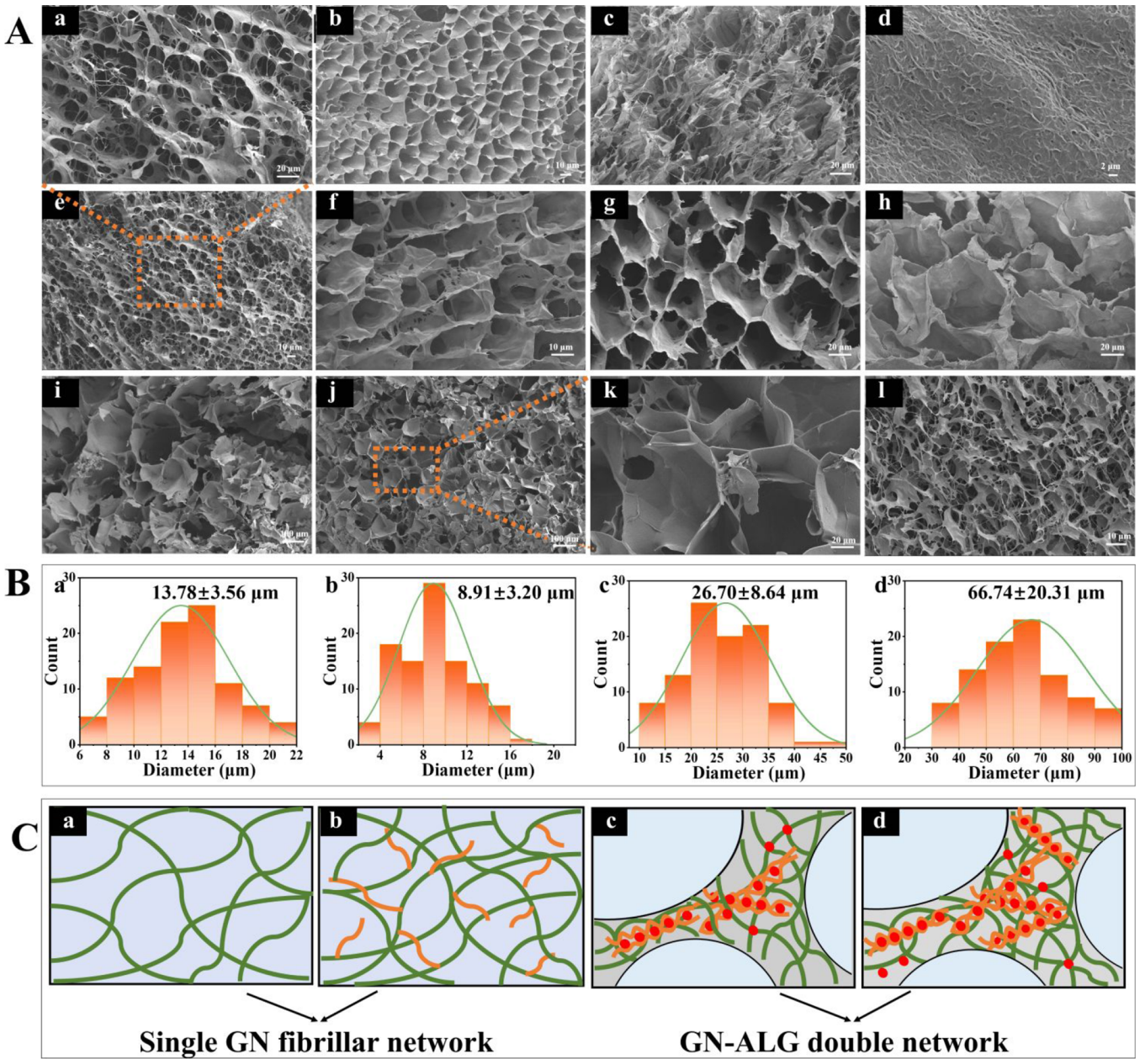

Figure 2. (A) FE-SEM images of hydrogels with the single fibrillar network: (b) 1% GN hydrogel, (c) 1% ALG solution and (d) the corresponding Ca^{2+}-cross-linked ALG hydrogel, and the GN-ALG-SN hydrogels with 1% GN and different ALG concentrations (a and e: 0.4%, l: 1%). FE-SEM images of GN-ALG-DN hydrogels with 1% GN and 0.4% ALG, cross-linked by (f) 0.5%, (g) 1%, and (h) 5% $CaCl_2$ solutions, and the hydrogels of 1% GN with (i) 0.6%, and (j and k) 1% ALG, cross-linked by 5% $CaCl_2$ solution. (B) Pore size and (C) the corresponding schematic network structure of (a) 1% GN hydrogel, (b) GN-ALG-SN hydrogel with 0.4% ALG, (c) GN-ALG-DN hydrogel with 0.4% ALG, treated by 1% $CaCl_2$, and (d) GN-ALG-DN hydrogel with 1% ALG, treated by 5% $CaCl_2$.

hydrogels (Figure 1Aa,b). Compared to GN hydrogel, the GN-ALG-SN hydrogels, especially with a higher ALG concentration (e.g., 0.6−1%), have a more turbid appearance and higher values of viscoelastic moduli (Figures 1Ba and S1A,B, Supporting Information), suggesting that the presence of ALG within GN network can efficiently increase hydrogel strength. However, these obtained GN-ALG-SN hydrogels still show a relatively low mechanical performance, which means they are not able to retain the desired shape (Figure 1Ba).

We then introduced the secondary network (i.e., Ca^{2+}-cross-linked ALG network) into the first GN fibrillar network by diffusing Ca^{2+} into the preformed GN-ALG gel matrix (Figure 1Ac), in which the Ca^{2+} can simultaneously induce the generation of new ALG network and enhance the GN fibrillar network. This thus leads to the formation of GN-ALG hydrogels with a unique interpenetrating DN that comprises the Ca^{2+}-enhanced self-assembled hydrogen-bond GN network and the Ca^{2+}-cross-linked ALG gel network. For comparison, the hydrogels with a single GN fibrillar network including Ca^{2+}-enhanced GN hydrogel (GN-SN) and the Ca^{2+}-cross-linked ALG hydrogel (ALG-SN) as control samples were also obtained, respectively. For the ALG-SN hydrogel, Ca^{2+} induces the quick formation of an ALG-Ca^{2+} "egg-box" network, forming an irregular and unshaped gel (Figure S2A, Supporting Information). In the presence of Ca^{2+}, the appearance of GN-SN hydrogel becomes cloudier than GN hydrogel without Ca^{2+}

https://doi.org/10.1021/acsami.3c10407
ACS Appl. Mater. Interfaces 2023, 15, 43633−43647

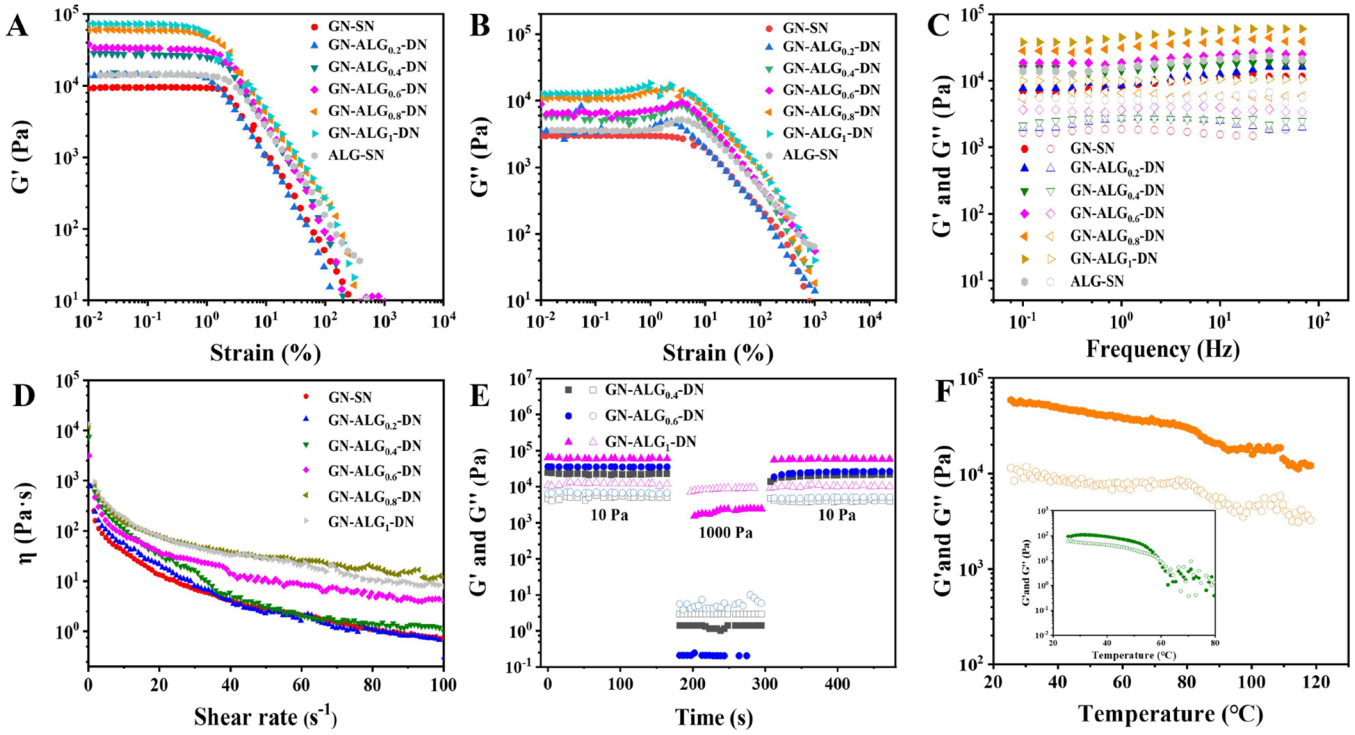

Figure 3. (A and B) Strain amplitude and (C) frequency sweeps, and (D) viscosity curves of Ca^{2+}-enhanced 1% GN hydrogel (GN-SN), Ca^{2+}-cross-linked 1% ALG hydrogel (ALG-SN), and the GN-ALG-DN hydrogels with 1% GN and different ALG concentrations (0.2−1%), immersed in 5% $CaCl_2$ solution. (E) Thixotropic recovery of the GN-ALG-DN hydrogels with 0.4, 0.8, and 1% ALG (GN-$ALG_{0.4}$-DN, GN-$ALG_{0.8}$-DN, and GN-ALG_1-DN, respectively); 10 and 1000 Pa mean the low stress within the LVR and the high stress beyond the LVR applied in the test, respectively. (F) Temperature sweeps of the GN-ALG_1-DN hydrogel and the corresponding GN-ALG_1-SN hydrogel (inset image). G' and G'' are shown as filled and open symbols, respectively.

(Figure 1Bb). This is related to the fact that the presence of Ca^{2+} will reduce the electrostatic repulsion, which can strengthen the hydrogen bond interactions within the GN−GN mixtures and thus increases the extent of interfibrillar aggregation. It is noted that both the ALG-SN and GN-SN hydrogels show a low shaping ability and can be easily fractured after compression (Movie 1, Supporting Information), which is related to their relatively weak gel structure. Interestingly, in comparison with the GN-ALG-SN hydrogels (Figures 1Ba and S1A,B, Supporting Information), the corresponding GN-ALG-DN hydrogels show a more solid appearance and significantly higher viscoelastic moduli (Figures 1Bb and S1C, Supporting Information), suggesting that the presence of Ca^{2+}-cross-linked ALG network and Ca^{2+}-enhanced GN network in GN-ALG matrix can together improve hydrogel strength. These structured and shaped GN-ALG-DN hydrogels can recover the gel structures to the initial state after large compression, further indicating their high gel strength (Figure 1Bb and Movie 2, Supporting Information). Taken together, these results demonstrate the successful fabrication of GN-ALG-DN hydrogels with a high shape stability and excellent mechanical performance.

3.2. Structural Properties of GN-ALG-DN Hydrogels. *3.2.1. Interactions within the Hydrogels.* To investigate the GN-GN, GN-ALG, and ALG-ALG interactions within these interpenetrating DN hydrogels, we then carried out FTIR measurements on the hydrogels after freeze-drying (Figures 1C,D). As shown in Figure 1C, a dominant and broad O−H stretching zone between 3550 and 3200 cm^{-1} can be observed in the GN hydrogel without Ca^{2+} (i.e., GN), suggesting the formation of interfibrillar hydrogen bonds. The other main peaks at 2945, 2872, 1727, 1363, 1263, 1170, and 1042 cm^{-1} were also detected in GN hydrogel, which is related to the CH_2 antisymmetric stretching, C−H symmetric stretching of CH_3 groups, C═O stretching, C−H bending of CH_3 groups, C−O stretching, C−O−C stretching, and C−O stretching, respectively.[30] After introducing Ca^{2+} in GN hydrogel (i.e., GN-SN), a slight hydroxyl stretching shift from 3447 to 3442 cm^{-1} was observed, suggesting that the presence of Ca^{2+} can enhance interfibrillar hydrogen-bond interactions, which is in good agreement with our previous studies.[30,31] In the ALG-SN hydrogel, the stretching vibration of the O−H groups at 3421 cm^{-1}, C−O bending near 1050 cm^{-1}, and the asymmetric and symmetric stretching vibration of the −COOH groups at the peaks of 1624 and 1433 cm^{-1}, can be found. Moreover, the presence of the peak at 822 cm^{-1} confirms the formation of the Ca^{2+}-ALG linkage.[36] For the spectra of GN-ALG-DN hydrogels, all characteristic peaks of GN and ALG can be observed (Figure 1C,D). It is noted that, in comparison with the stretching vibration of the O−H groups of the GN-SN hydrogel at 3442 cm^{-1}, the ALG-SN hydrogel at 3421 cm^{-1}, and their physical mixtures at 3441 cm^{-1}, the O−H stretching peak of the GN-ALG-DN hydrogels with the same GN and ALG concentration is shifted to a lower wavenumber of 3405 cm^{-1}, which confirms the formation of an intermolecular hydrogen bond between GN and ALG. Based on the above results, it can be concluded that the interpenetrating DN is mainly driven by the multiple intramolecular (GN-GN and ALG-ALG) and intermolecular (GN-ALG) hydrogen bonds, as well as ALG-Ca^{2+} ionic bonds. Note that the result of XRD indicates that GN-ALG-DN hydrogels maintain the initial crystallographic structure of GN-SN and ALG-SN hydrogels

https://doi.org/10.1021/acsami.3c10407
ACS Appl. Mater. Interfaces 2023, 15, 43633−43647

(Figure 1E), indicating that the interactions between GN and ALG do not affect the structures of GN and ALG.

3.2.2. Microstructure of Hydrogels. The microstructures of the above-obtained GN-based hydrogels were observed by FE-SEM. As can be seen in Figure 2Ab, the GN hydrogel without Ca^{2+} shows a homogeneous and interconnected 3D porous structure with a pore size of around 13.78 μm (Figure 2Ba,Ca). The ALG solution exhibits a flaky structure due to the absence of 3D networks, and after the addition of Ca^{2+}, the formed ALG hydrogel possesses a dense and wrinkled film structure (Figures 2Ac,d). The structural complexity and compactness of the GN-ALG-SN hydrogels by incorporating ALG into the GN network are significantly enhanced, especially with a higher ALG concentration of 1% (Figure 2Aa,e,l), which can be explained by the fact that the ALG polymer chain interpenetrates into the self-assembled GN fibrillar network architecture, thus reinforcing the gel matrix through hydrogen bond interactions (Figure 2Bb,Cb), which is in good agreement with the results of the appearance and rheological properties of GN-ALG-SN hydrogels (Figures 1Ba and S1A,B, Supporting Information). Upon the introduction of Ca^{2+} into the GN-ALG-SN hydrogels, the obtained GN-ALG-DN hydrogels display an obviously strengthened gel network with a larger pore size (~30 μm) and a thicker pore wall (Figures 2Af–k,Bc,d). This is more evident with increasing Ca^{2+} and ALG concentrations, which is in accordance with the appearance and rheological properties of these hydrogels (Figures 1Bb and S1C, Supporting Information). When the Ca^{2+} diffuses into the preformed first GN-ALG network matrix, it not only induces the generation of the ALG-Ca^{2+} "egg-box" network, but also can promote the aggregation of GN fibrillar network, leading to the formation of a unique interpenetrating DN that comprises the Ca^{2+}-enhanced self-assembled hydrogen-bond GN network and the Ca^{2+}-cross-linked ALG gel network, thus constituting the robust gel skeleton between large pores (Figures 2Cc,d). These results together clearly indicate that the microstructure of the GN-ALG-DN hydrogels largely depends on the multiple interactions among GN-GN, GN-ALG, and ALG-Ca^{2+}, which are related to the structural formation and stability of hydrogels as well as their mechanical properties, as discussed in the following section.

3.3. Rheological Properties of GN-ALG-DN Hydrogels.

3.3.1. SAOS. The dynamic oscillatory shear test, including SAOS and LAOS, is widely used as a powerful tool to analyze the microstructural changes and mechanical response of various soft materials (e.g., hydrogels) during deformation. We first studied the structural viscoelasticity of GN-ALG-DN hydrogels by performing a SAOS test, including oscillatory amplitude and frequency sweep measurements. The strain sweeps of GN-ALG-DN hydrogels with a constant GN concentration (1%) and different ALG concentrations (0–1%) are shown in Figure 3A,B. For all hydrogels, the elastic modulus (G') is always significantly higher than the viscous modulus (G'') in their LVRs, suggesting the mostly elastic solid-like behavior. In the G' curve (Figure 3A), all hydrogels have a plateau at small strain amplitudes (within the LVR), followed by a decrease at higher strain amplitudes. Compared to the GN-SN hydrogel (G' = 14865 Pa, in the LVR), the GN-ALG-DN hydrogels display significantly higher G' values of 15640–65410 Pa (Table S1, Supporting Information). In the G'' curve (Figure 3B), the GN-SN hydrogel exhibits a typical strain thinning behavior (Type I), showing a decrease as the strain increases beyond the LVR. In contrast, the GN-ALG-DN hydrogels and ALG-SN hydrogels show an overshoot in G'', followed by a sudden decrease, which is a feature of soft glassy materials and suggests that these gels can be classified as type III materials. The overshoot behavior can be attributed to the simultaneous destruction and reformation of the ALG network junctions.[32,37] In addition, with increasing ALG concentration, the values of G' and G'' significantly increase, indicating the contribution of the secondary Ca^{2+}-cross-linked ALG network to the gel strength. These results are supported by the frequency sweeps of the hydrogels (Figure 3C). Further, power-law model equations of G' and G'' against frequency were used to analyze the frequency dependence of the GN-ALG-DN hydrogels (Table S1, Supporting Information). As can be seen, for all hydrogels, both G' and G'' curves have slightly positive slopes ($0.17 < n' < 0.23$, $n'' < 0.1$), suggesting that the rheological response of the hydrogels is not largely affected by applied deformation rate.[32,38] The damping factor, tan δ (G''/G'), is often used to express the contribution of the elastic and viscous parts to the viscoelastic response of materials. The tan δ is equal to 0 or 1 and means a perfectly elastic or viscous material, respectively. Compared to the hydrogels of pure GN (tan δ = 0.54), the GN-SN (tan δ = 0.32), and the ALG-SN (tan δ = 0.31), the GN-ALG-DN hydrogels show a significantly lower damping factor (around 0.2) (Table S1, Supporting Information), which suggests the enhanced elasticity of these hydrogels due to their DN structure. These results indicate that the GN-ALG-DN hydrogels are highly elastic soft materials, and the interpenetrating DN (Figures 1Bb and 2Af–k,Cc,d) mainly contributes to their superior rheological properties.

The steady-state flow properties of the GN-ALG-DN hydrogels were then measured. As can be seen in Figure 3D, the viscosities of all hydrogels decrease with increasing shear rate from 0.1 to 100 s^{-1}, indicating a typical shear-thinning behavior due to the shear-induced network destruction. Compared to the GN-SN hydrogel, the GN-ALG-DN hydrogels, especially those with higher ALG concentrations (0.8 and 1%), show significantly higher η values, suggesting a higher gel network strength. To gain insight into the structural-recovery properties of the GN-ALG-DN hydrogels, we further studied their thixotropic behavior by using a three-interval time test, where the G' and G'' of hydrogels were monitored as a function of time under an alternate cycle of low stress (10 Pa, within the LVR) and high stress (1000 Pa, beyond the LVR). As shown in Figure 3E, for all GN-ALG-DN hydrogels, there are no obvious changes in G' and G'' values at the low-stress (10 Pa, $G' > G''$) in the first interval. When the stress increases from 10 to 1000 Pa in the second interval, both moduli decrease sharply, and the G'' exceeds G', which suggests the structural damage of the gel network under large deformation (beyond yield stress). As the stress goes back to 10 Pa, both moduli can recover to their initial values, revealing that the network structure is well restored. The structure recovery degree of the hydrogels was then quantitatively analyzed by comparing the maximum G' value in the third interval and the minimum G' value in the first interval. The recovery percentage of these hydrogels was 75.31–98.80%, indicating the high structure recovery ability of GN-ALG-DN hydrogels. We also evaluate the thermal stability of the GN-ALG-DN hydrogels, since previous studies reported that the GN supramolecular hydrogels are thermally reversible and have a gel–sol transition temperature of around 55–60 °C.[26,29–32] As seen in Figure 3F, the GN-ALG-SN hydrogel exhibits a gel-to-

https://doi.org/10.1021/acsami.3c10407
ACS Appl. Mater. Interfaces 2023, 15, 43633–43647

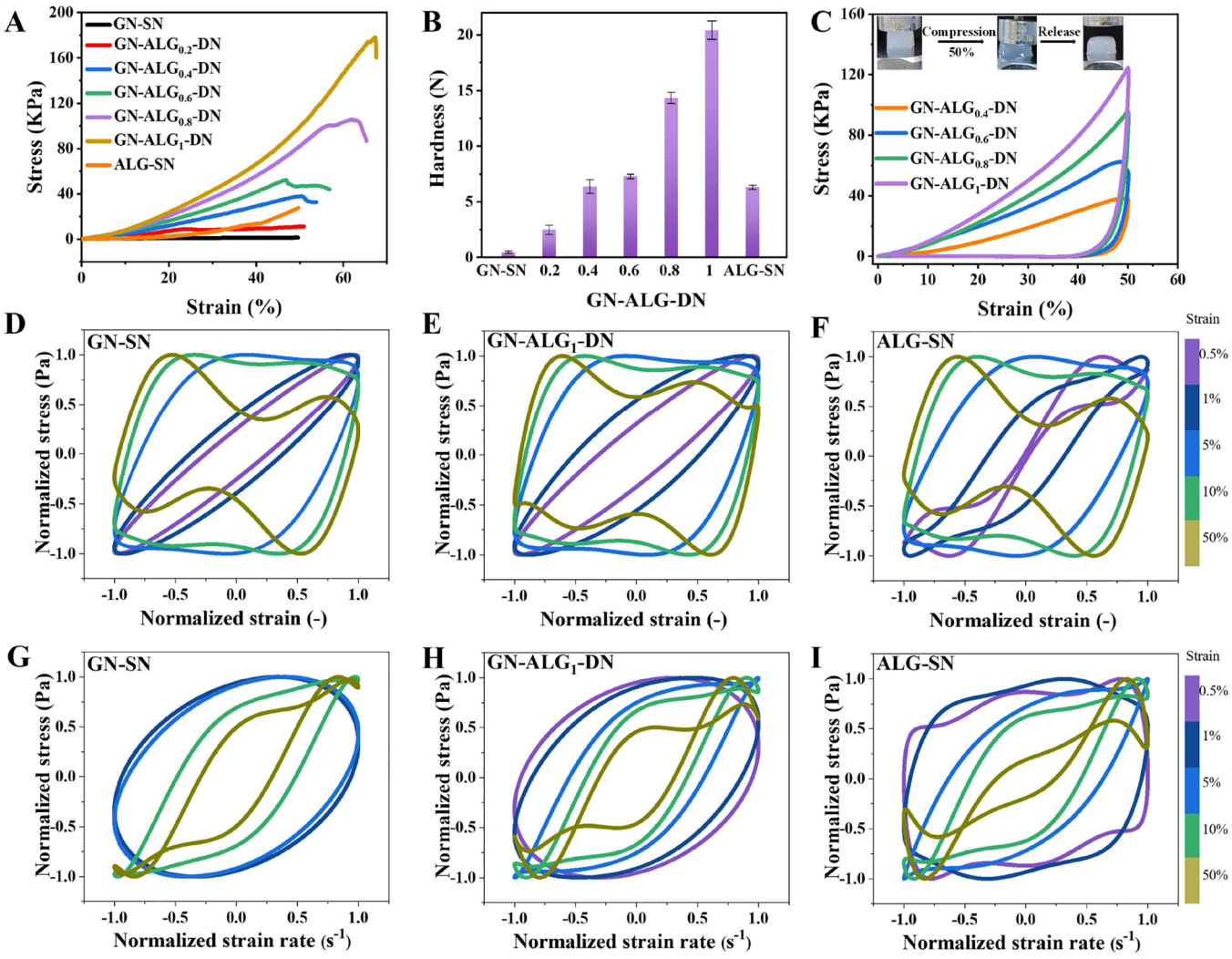

Figure 4. (A) Large deformation compression strain−stress curves, (B) maximum hardness, and (C) loading−unloading compression curves of the Ca^{2+}-enhanced 1% GN hydrogel (GN-SN), Ca^{2+}-cross-linked 1% ALG hydrogel (ALG-SN), and the GN-ALG-DN hydrogels with 1% GN and different ALG concentration (0.2−1%), immersed in 5% $CaCl_2$ solution. Inset photographs in (C) show the GN-ALG-DN hydrogel with 1% ALG before and after compression at 50% strain. (D−F) Elastic and (G−I) viscous normalized Lissajous−Bowditch plots of GN-SN, ALG-SN, and the GN-ALG-DN hydrogel with 1% ALG (GN-ALG_1-DN), obtained at the frequency of 1 Hz and different strains of 0.5, 1, 5, 10, and 50%.

sol phase transition ($G' = G''$) at about 58 °C during heating, which is due to the melting of the hydrogen-bond GN fibrillar network (see inset of Figure 3F).[26,29−32] It is worth noting that for the GN-ALG-DN hydrogels, the G' was always higher than G'' during heating (Figures 3F and S3, Supporting Information), suggesting that the formation of the interpenetrating DN structure endows the hydrogels with excellent thermal stability.

3.3.2. LAOS. Compared to the SAOS, the LAOS test, in which the strain amplitude is sufficiently high to evoke the nonlinear viscoelastic behavior, can provide more information about the mechanical response of materials during practical processing.[37,39−41] In particular, the elastic and viscous Lissajous−Bowditch curves decomposed from the shear stress waveform in each domain of the viscoelastic LAOS test, which shows the instantaneous intracycle stress of the material as a function of the applied strain or shear rate, can together provide useful information about their structural transitions and viscoelastic response under large deformation. It is known that the strain amplitude has no impact on the elastic and viscous moduli of materials within the LVR, in which the oscillatory stress response is sinusoidal and the Lissajous curve shows an elliptical shape. In contrast, in the nonlinear regime, the viscoelastic moduli largely depend on the imposed strain, and the existence of higher harmonics in the stress response results in distorted, nonsinusoidal shear stress waveforms.[39,42,43] Therefore, to further understand the GN-ALG-DN hydrogel network structure from a nonlinear rheological point of view, we compare the normalized Lissajous-Bowditch plots of GN-SN, ALG-SN, and GN-ALG-DN hydrogels, which are evaluated at different strains (0.5, 1, 5, 10, and 50%) and a fixed frequency (1 Hz). As can be observed in Figure 4D−I, the GN-SN and GN-ALG-DN hydrogels at a strain range from 0.5 to 1% (within the LVR) show a perfectly elliptical shape in the normalized elastic and viscous Lissajous-Bowditch curves. Moreover, the decomposed elastic and viscous stresses are straight lines with a slope equal to G' and $\eta' = G''/\omega$, respectively (Figures S4 and S5, Supporting Information). This confirms that the total stress is closer to the decomposed elastic stress, indicating a linear viscoelastic solid-like behavior (predominantly elastic). This is in good agreement with the results of the SAOS tests (Figures 3A,B). Upon increasing the

https://doi.org/10.1021/acsami.3c10407
ACS Appl. Mater. Interfaces 2023, 15, 43633−43647

strain above the LVR (>1%), especially at the strain range of 10−50%, the normalized elastic and viscous Lissajous curve shapes are shifted to a near parallelogram shape and a near S-shape, respectively, suggesting an increase of viscous dissipation during intracycle deformation and a final shift from elastic- to viscous-dominated behavior with strong shear-thinning at higher strain rates. The observed specific shape distortions of the normalized Lissajous curves with increasing strain are largely related to the microstructural changes and responses of hydrogels under large deformations, which exhibit elastic straining (1−5% strain) and yielding behavior (10−50% strain). It is worth noting that, for the GN-ALG-DN hydrogel, a continuous upturn of the decomposed elastic and viscous stresses is observed in the strain range between 0.5 and 5%. In contrast, the ALG-SN hydrogel exhibits a yielding behavior at a very low deformation of 0.5% (Figures S4 and S5, Supporting Information), which is due to its brittleness property and suggests that the higher concentration of ALG (e.g., above 1%) in the GN-ALG-DN hydrogels may lead to a lower ability to resist large deformations. More importantly, from the elastic and viscous Lissajous curves, the GN-ALG-DN hydrogel shows lower distortion from their original shape and smaller enclosed area of the loops with increasing strain, as compared to those of the ALG-SN hydrogel, which suggests that the microstructure of the GN-ALG-DN hydrogels is more elastic and thus has higher ability to resist large deformations, leading to a lower extent of nonlinear response. Moreover, the normalized viscous Lissajous curves of the ALG-SN and GN-ALG-DN hydrogels show the secondary loops at a higher strain of 10%, which cannot be observed in the GN-SN hydrogel, in good accordance with the stress overshoot in G'' curves (Figure 3B). This is related to the fact that the time scale for the microstructure rearrangement of the pure ALG "egg-box" network is shorter than that for the deformation.[32,40] The above results together indicate that the GN-ALG-DN hydrogel possesses a high structural elasticity and an excellent ability to resist large deformations, which is mainly attributed to the GN fibrillar network within the gel matrix, providing a slow relaxation process mediated by the interfibrillar hydrogen bonding interactions.

To quantitatively evaluate the nonlinear response of these hydrogels, we then compare the intracycle nonlinear parameters from the Lissajous plots, including the stiffening ratio (S factor) and thickening ratio (T factor). As shown in Figure S6A, at a small strain amplitude in the range of 0.5−1%, the S factor of the GN-ALG-DN hydrogel is close to zero, illustrating no intracycle elastic nonlinearity, which is in good agreement with the Lissajous plots (Figure 4D−I). With increasing amplitude (1−50%), the S factor values gradually increase and remain positive, suggesting a nonlinear intracycle strain stiffening of the elastic response. It is worth noting that for the GN-ALG-DN hydrogel, the changing trend of the S factor with strain amplitudes is similar to that of the GN-SN hydrogel, which implies that the nonlinear elasticity in the form of strain stiffening is most likely attributed to the increasing contacts between the semiflexible GN nanofibrils within the gel network, thus inducing the transition from a bending-dominated to a stretching-dominated deformation. Similar behaviors of intracycle strain stiffening have been reported in these hydrogels with fibrin or filamentous protein networks.[41,44,46] In addition, at 50% strain, the S factor values for the GN-ALG-DN and GN-SN hydrogels are significantly lower than those of the ALG-SN hydrogel, suggesting a lower degree of nonlinearity, which further confirms the greater ability of the GN fibrillar network to resist large deformations. This is in good agreement with the results of Lissajous plots and linear SAOS rheology (Figures 3A,B, and 4D−I). Further, at relatively low amplitude (0.5−10%), the positive T factor values of all hydrogels reveal a nonlinear intracycle shear thickening of viscous response (Figure S6B, Supporting Information), which is due to the formation of a temporary structure within hydrogels under shear-induced alignment by enhancing the molecular interactions.[41,47,48] However, at the large strain of 50%, the intensity of intracycle shear thickening is reduced and even transformed into a shear thinning behavior, especially for the ALG-SN hydrogel (Figure S6B, Supporting Information). This implies that the gel network is broken and becomes more fluid by a large shearing at higher strains, which is related to the fact that the reformation of physical interactions is postponed due to the insufficient time for relaxation under high deformation amplitudes (i.e., 50% strain), further supporting the greater ability of the GN-ALG-DN hydrogel to respond to large shear deformations.

3.4. Large Deformation Compression Properties of GN-ALG-DN Hydrogels. The large deformation compression test was further carried out to illustrate the compressibility of GN-ALG-DN hydrogels. Figure 4A,B show the stress−strain curves and the maximum hardness of the hydrogels under large deformation compression, respectively. As shown in Figure 4A, compared to the GN-ALG-DN hydrogels, the GN-SN and ALG-SN hydrogels show lower stress values due to their weak network structure and limited shaping ability (Figures 1Bb, 2Ad, and S2A, Supporting Information). It is expected that the fracture strain, fracture stress, maximum hardness, and Young's modulus values of the GN-ALG-DN hydrogels significantly increase with an increasing ALG concentration (Figure 4B and Table S2, Supporting Information). The GN-ALG-DN hydrogel with 1% ALG can withstand compression without obvious breakage until 65.69% strain, and shows the highest values of hardness (20.41 N) and Young's modulus (88.85 kPa), which are 8.30 and 16.76 times of those in the GN-SN hydrogel (i.e., 2.46 N and 5.30 kPa), respectively. This suggests that the mechanical properties of the GN-ALG-DN hydrogels can be enhanced by increasing the ALG concentration, which is in good agreement with the SAOS rheological results (Figure 3A−C). The one cyclic loading−unloading curve with 50% strain for the GN-ALG-DN hydrogels (0.4−1% ALG) is shown in Figure 4C. As can be seen, for all hydrogels, the unloading path differs from the loading curve, showing a hysteresis loop, which indicates the energy dissipation of the hydrogels. The inset images in Figure 4C further visually display that the GN-ALG-DN hydrogel (1% ALG) can mostly return to its original shape without breakage after the loading−unloading cycle for one time at 50% strain, demonstrating the compression stability with partial energy dissipation. This is related to the fact that the GN fibrillar network serves as sacrificial bonds to efficiently dissipate energy, and the fast, ordered GN assembly makes the gel network reform quickly when the mechanical load is released. These results obtained from the SAOS, LAOS, and large deformation compression tests (Figures 3, 4, and S4−S6, Supporting Information), together reveal that the GN-ALG-DN hydrogels possess the combined advantages of the individual GN and ALG gel networks, including the high ability to resist large deformations of the GN fibrillar network and the high mechanical strength of the ionic-cross-linked ALG polymer network, which can endow these hybrid DN

https://doi.org/10.1021/acsami.3c10407
ACS Appl. Mater. Interfaces 2023, 15, 43633−43647

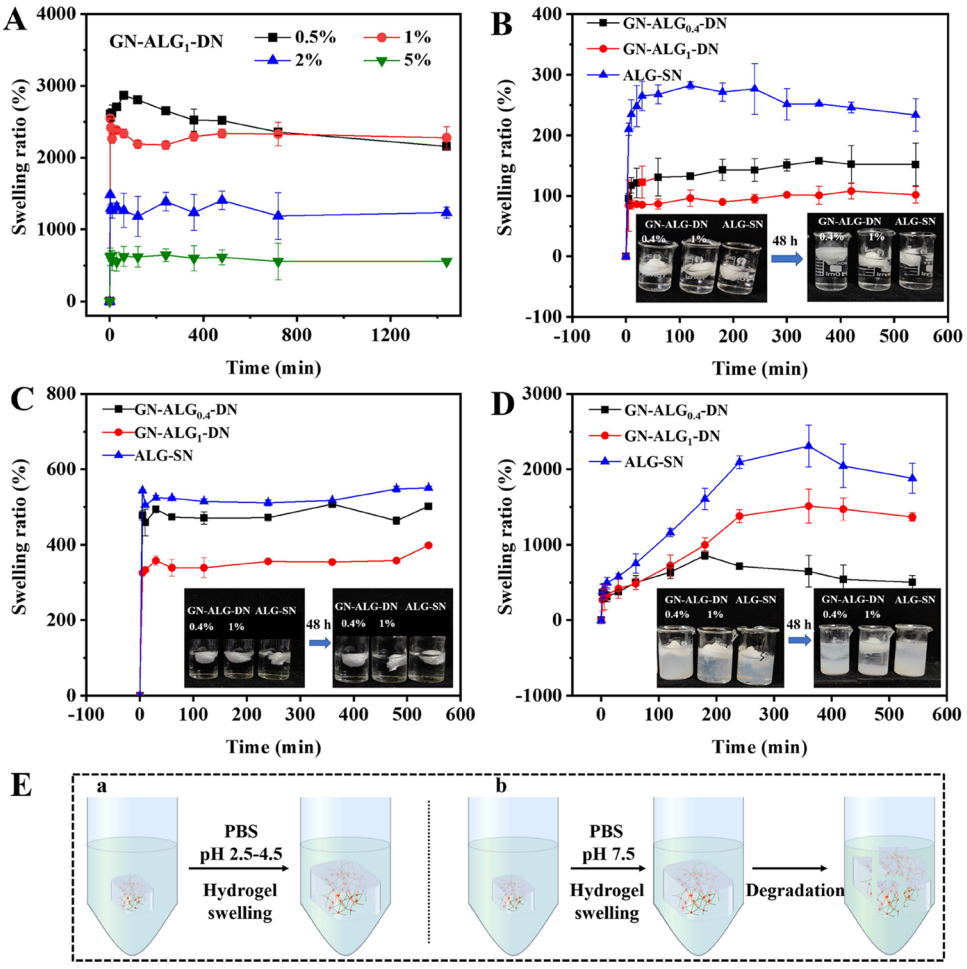

Figure 5. (A) Swelling ratio of the GN-ALG-DN hydrogel with 1% ALG (GN-ALG$_1$-DN) as a function of time, treated with different concentrations of $CaCl_2$ solutions (0.5, 1, 2, and 5%). Swelling curves of Ca^{2+}-cross-linked 1% ALG hydrogel (ALG-SN) and GN-ALG-DN hydrogels with 0.4 and 1% ALG (GN-ALG$_{0.4}$-DN and GN-ALG$_1$-DN, respectively) in PBS solutions with different pH values: (B) 2.5, (C) 4.5, and (D) 7.5; inset images show the appearances of these hydrogels before and after swelling for 48 h. (E) Schematic diagram of GN-ALG-DN hydrogels after immersion in PBS solutions with different pH values (a: pH 2.5 and 4.5; b: pH 7.5).

hydrogels with adequate mechanical strength and advanced functional performance for a variety of applications.

3.5. Swelling Properties of GN-ALG-DN Hydrogels. The swelling property of hydrogels is one of the critical parameters affecting the diffusion and release rates of loaded bioactives or nutrients. As shown in Figure S7A (Supporting Information), pure GN hydrogel (without Ca^{2+}) disappears quickly (within 1 min) after immersion in water, showing a rapid dissolution. The addition of ALG can enhance the structural stability of the GN-ALG-SN hydrogel, whereas it still completely decomposes when immersed in water for 40 min (Figure S7B, Supporting Information), which suggests the rapid swelling and subsequent dissolution behavior of the dried GN and GN-ALG-SN hydrogels with only a single GN fibrillar network. After the introduction of Ca^{2+} (0.5−5%), the obtained shaped, dried GN-ALG-DN hydrogels can maintain satisfactory structural stability with a swelling ratio in the range of 500−3000% (Figures 5A and S2B, Supporting Information), and the increase of Ca^{2+} concentration decreases the swelling degree significantly due to the increased gel network compactness (Figure 2Af−h), which facilitates increasing the swelling resistance ability.

We then evaluated the swelling properties of the ALG-SN and GN-ALG-DN hydrogels in PBS solutions with different pH values of 2.5, 4.5, and 7.5. As shown in Figure 5B−D, for all cases, as expected, the initial swelling rate and the equilibrium swelling ratio of the GN-ALG-DN hydrogels are lower than those of the ALG-SN hydrogel, and the increase of ALG concentration also can reduce the swelling degree of the GN-ALG-DN hydrogels. Further, it can be clearly seen that the pH values of the swelling medium have a significant effect on the swelling behavior of hydrogels, which depend strongly on the acidic and basic conditions of the solution medium. For the medium with acidic pH values (2.5 and 4.5), the hydrogels exhibit a rapid initial swelling within a few minutes and then reach a swelling plateau (Figure 5B,C). After that, these swollen hydrogels can remain stable even after immersion in solutions for 48 h (see the inset images of Figure 5B,C). In contrast, at a basic medium (pH 7.5), after the initial swelling, the swelling ratios of these hydrogels further increase dramatically with time, reaching a very high swelling ratio of about 2308.96% at 360 min. However, it is noted that these hydrogels at pH 7.5 exhibit a consequent degradation behavior with a continuously decreased swelling ratio, and their structural compactness is destroyed and partially degraded into several pieces (Figure 5D). The pH-dependent swelling behavior of the GN-ALG-DN hydrogels can be related to the dissociation degree of carboxylic groups in GA and ALG

https://doi.org/10.1021/acsami.3c10407
ACS Appl. Mater. Interfaces 2023, 15, 43633−43647

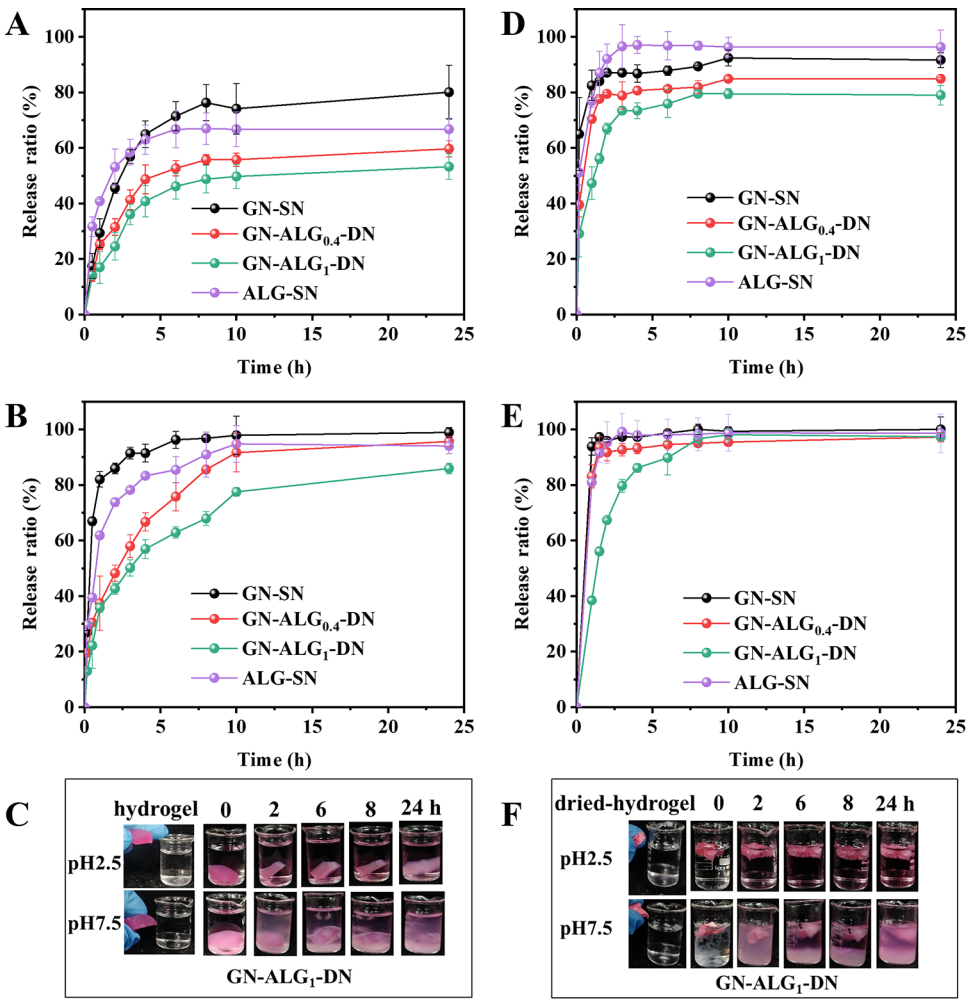

Figure 6. Release profiles of a model nutrient (VB_{12}) at 25 °C from wet 1% GN hydrogel (GN-SN), 1% ALG hydrogel (ALG-SN), and the GN-ALG-DN hydrogels with 0.4 and 1% ALG (GN-$ALG_{0.4}$-DN and GN-ALG_1-DN, respectively), obtained in PBS solutions with pH (A) 2.5 and (B) 7.5, respectively. Release of VB_{12} from these corresponding freeze-dried hydrogels in PBS solutions with pH (D) 2.5 and (E) 7.5. Photographs show the appearances of the (C) wet and (F) freeze-dried GN-ALG-DN hydrogels with 1% ALG (GN-ALG_1-DN) during the release process of VB_{12} in PBS solutions at pH 2.5 and 7.5.

molecules. At acidic pH values (2.5 and 4.5), the self-assembled GN and the resultant GN fibrillar network are structurally stable in the DN matrix, especially at pH 2.5, where the protonation of the carboxyl groups in GA and ALG molecules weakens the electrostatic repulsion within the system, further enhancing the compactness and stability of the gel network and thus decreasing the swelling degree (Figure 5B,C,E). However, at a basic pH (7.5), the complete dissociation of the carboxyl groups can lead to the gradual erosion and destruction of the GN fibrillar network and ionic-cross-linked ALG network, which thus results in the high swelling degree and subsequent degradation of hydrogels (Figures 5D,E).

3.6. In Vitro pH-Responsive Nutrient Release of GN-ALG-DN Hydrogels. Stimuli-responsive hydrogels have been widely used as the delivery platform to achieve spatial and temporal control over the release of various nutrients and bioactive cargoes.[14,45] Here, we investigated the release behaviors of hydrophilic bioactive compounds (i.e., VB_{12}) within the GN-ALG-DN hydrogel under PBS mediums at pH 2.5 and 7.5, respectively. As expected, in all cases, the release rate and release content of VB_{12} in the GN-ALG-DN hydrogels are lower than those in the GN-SN and ALG-SN hydrogels, and the increase in ALG concentration can reduce the VB_{12} release (Figure 6A,B). It is worth noting that the GN-SN and ALG-SN hydrogels show a burst release of VB_{12} within 1 h, which is more evident in the PBS solution with a basic pH (7.5), reaching the release ratio of 82.00 and 61.83%, respectively. After that, these two hydrogels display a slow release and then reach a relative equilibrium state within 4 h under both acidic and basic conditions. In contrast, for the GN-ALG-DN hydrogels, the initial VB_{12} release within 1 h is significantly lower with a release ratio of 17.02 and 35.76% under pH 2.5 and 7.5, respectively, and a further slow and sustained release of VB_{12} is observed in the subsequent incubation (within 10 h). These results suggest that the combination of the Ca^{2+}-enhanced supramolecular GN network and the Ca^{2+}cross-linked ALG polymer network can efficiently prevent the burst release of VB_{12}, endowing the hydrogels with a superior ability to release bioactives in a sustained and controlled manner. Moreover, the VB_{12} release profiles for the GN-ALG-DN hydrogels under acidic (pH 2.5) and basic (pH 7.5) conditions are significantly different, showing a pH-responsive controlled release property. As seen, a relatively small proportion of VB_{12} (<50%) is released from the hydrogel at pH 2.5 (Figure 6A). Throughout the period

https://doi.org/10.1021/acsami.3c10407
ACS Appl. Mater. Interfaces 2023, 15, 43633−43647

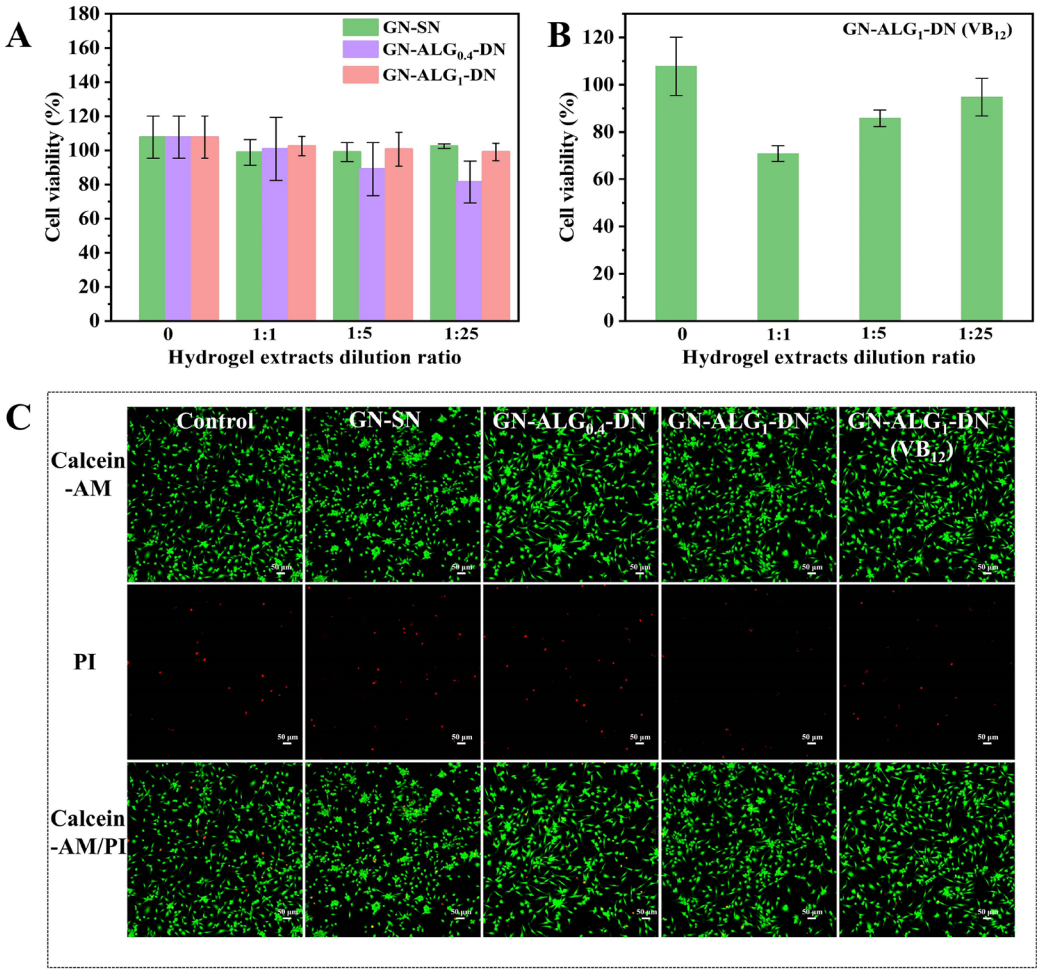

Figure 7. Cell viability of L929 after 24 h of incubation with the diluted solutions of (A) GN-ALG-DN hydrogel extracts and (B) the VB_{12}-loaded GN-ALG-DN hydrogel extracts. "GN-SN" means the Ca^{2+}-enhanced 1% GN hydrogel. (C) Live−dead fluorescence staining images of L929 cells incubated with these hydrogel extract liquids (20 mg/mL) for 24 h; the live cells were stained by Calcein-AM with green fluorescence, and the dead cells were stained by Propidium Iodide (PI) with red fluorescence.

studied (24 h), the GN-ALG-DN hydrogels at pH 2.5 remain structurally stable and compact (Figure 6C), and thereby, the intact interpenetrating DN structure can prolong the diffusion pathway of VB_{12} and efficiently inhibit its release. In contrast, at pH 7.5, the GN-ALG-DN hydrogels are destroyed and partially degraded into several pieces during the release process, which displays a sustained VB_{12} release with a higher release ratio of 85.90% within 24 h (Figure 6B,C). At basic pH, the complete dissociation of carboxyl groups in GA and ALG molecules induces the erosion and destruction of the GN fibrillar network as well as the Ca^{2+}-cross-linked ALG network, ultimately resulting in the gel degradation and a high VB_{12} release profile.

The VB_{12} release profiles from the dried samples of these aforementioned hydrogels were further investigated. Compared to the wet hydrogels (Figure 6A−C), the dried samples show a significantly higher initial release rate and equilibrium release ratio of VB_{12} (Figure 6D−F), which is related to their greater swelling degree (Figure 5B,D). In particular, the dried GN-SN and ALG-SN hydrogels at pH 7.5 have an exaggerated burst-release behavior with high release ratios of 93.85 and 80.96% within 1 h, respectively. However, for the GN-ALG-DN hydrogels, the high swelling resistance property and the increased gel network compactness (Figures 2Af−k and 5B−D, especially the GN-ALG_1-DN) impart the dried hydrogels with the high inhibition effect for VB_{12} diffusion, showing a lower initial release ratio of about 40% within 1 h. In addition, the GN-ALG-DN hydrogels also exhibit a higher VB_{12} release profile at pH 7.5 than at pH 2.5, as expected, further confirming the pH-responsive controlled active cargo release property. Taken together, these results indicate that the GN-ALG-DN hydrogels are an all-natural, efficient delivery platform with remarkable pH-responsiveness for the controlled release of a variety of nutrients and bioactives.

3.7. Biocompatibility of GN-ALG-DN Hydrogels.

Biocompatibility is an important parameter for the application of hydrogels. The biocompatibility of the GN-ALG-DN hydrogels against L929 fibroblasts was then examined using the MTT assay. To evaluate the cell viability of hydrogels with and without the loading of VB_{12}, the hydrogel extracts with different dilution ratios (1:1, 1:5, and 1:25) were used to incubate the L929 fibroblasts for 24 h. As seen in Figure 7A,B, no obvious differences in cell viability can be found between the control sample (without hydrogels) and the samples treated with different dilutions of hydrogel extracts, indicating that the hydrogel extracts have no observed effects on cell viability. After the loading of VB_{12}, the cell viability values slightly decrease but still remain above 70%, which points to

https://doi.org/10.1021/acsami.3c10407
ACS Appl. Mater. Interfaces 2023, 15, 43633−43647

the good cytocompatibility of the VB_{12}-loaded bioactive GN-ALG-DN hydrogels. For all GA-based hydrogels, the bright green fluorescence-specific labeling of live cells and the red fluorescence-specific labeling of dead cells are observed (Figure 7C), further confirming the cytocompatibility of these hydrogels. Therefore, these results suggest that the GN-ALG-DN hydrogels, with or without the loading of VB_{12}, are biocompatible, which is beneficial for their potential applications in the functional food and biomedical fields.

4. CONCLUSIONS

In summary, through a multicomponent gel approach, we successfully developed a novel mechanically robust GA-based hydrogel with an interpenetrating DN that is composed of the Ca^{2+}-enhanced hydrogen-bond supramolecular GN network and the Ca^{2+}cross-linked ALG polymer network. The synergistic effect of the DN structure enables the hydrogels to have a stronger mechanical strength and shaping ability, better rheological and thixotropy recovery properties, higher large deformation resistance performance and thermal stability, lower swelling properties, and a sustained and controlled release of hydrophilic nutrients and bioactives (i.e., VB_{12}), as compared with those of the hydrogels (GN-SN, ALG-SN, and GN-ALG-SN) with only the single fibrillar network. More importantly, the swelling and dissolution behaviors of the GN-ALG-DN hydrogels strongly influence the release profiles of VB_{12}, showing a pH-responsive controlled release property. At an acidic medium (pH 2.5), the protonation of the carboxyl groups in GA and ALG molecules weakens the electrostatic repulsion within the system, which enhances the compactness and stability of the gel network and thus efficiently inhibits VB_{12} diffusion, leading to a relatively small proportion of released VB_{12} (below 50%) within 24 h. At basic pH condition of 7.5, the complete dissociation of carboxyl groups in GA and ALG molecules makes the GN-ALG-DN hydrogels have a high structure erosion and degradation, thus accelerating the diffusion of VB_{12} with a high release ratio of 85.90%. These findings are expected to provide insights for developing robust and multifunctional supramolecular hydrogels from natural drug-food homologous small molecules (e.g., GA), which can serve as an efficient stimuli-responsive active cargo delivery platform for sustainable applications in food and biomedical fields.

■ ASSOCIATED CONTENT

Supporting Information

The Supporting Information is available free of charge at https://pubs.acs.org/doi/10.1021/acsami.3c10407.

Yield strain, crossover strain, G' in the LVR, power-law exponent, and tan δ values for GN, GN-SN, ALG-SN, and GN-ALG-DN hydrogels; fracture strain, fracture stress, and Young's modulus of these hydrogels; strain amplitude and frequency sweeps of GN, GN-$ALG_{0.4}$-SN, and GN-ALG_1-SN hydrogels; frequency sweeps of GN-ALG_1-DN hydrogel treated by different concentrations of $CaCl_2$ solutions; photographs of wet ALG-SN and dried GN-ALG-DN hydrogels; temperature sweeps of GN-ALG-DN hydrogels; normalized elastic and viscous Lissajous-Bowditch plots and nonlinear S and T factors of GN-SN, ALG-SN, and GN-ALG_1-DN hydrogels; photographs of dried GN and GN-ALG_1-SN hydrogels after immersion in water (PDF)

Deformation compression of GN-SN, ALG-SN, and GN-ALG-DN hydrogels (MP4)

■ AUTHOR INFORMATION

Corresponding Author

Zhili Wan − *Laboratory of Food Proteins and Colloids, School of Food Science and Engineering, Guangdong Province Key Laboratory for Green Processing of Natural Products and Product Safety, South China University of Technology, Guangzhou 510640, China; Overseas Expertise Introduction Center for Discipline Innovation of Food Nutrition and Human Health (111 Center), Guangzhou 510640, China;* orcid.org/0000-0002-5865-4301; Email: zhiliwan@scut.edu.cn; Fax: (086) 20-87114263

Authors

Qing Li − *Laboratory of Food Proteins and Colloids, School of Food Science and Engineering, Guangdong Province Key Laboratory for Green Processing of Natural Products and Product Safety, South China University of Technology, Guangzhou 510640, China*

Xinke Yu − *Laboratory of Food Proteins and Colloids, School of Food Science and Engineering, Guangdong Province Key Laboratory for Green Processing of Natural Products and Product Safety, South China University of Technology, Guangzhou 510640, China*

Shiqi Zhang − *Laboratory of Food Proteins and Colloids, School of Food Science and Engineering, Guangdong Province Key Laboratory for Green Processing of Natural Products and Product Safety, South China University of Technology, Guangzhou 510640, China*

Mengyue Xu − *Laboratory of Physics and Physical Chemistry of Foods, Wageningen University, Wageningen 6708WG, The Netherlands*

Yunyi Yang − *Laboratory of Food Proteins and Colloids, School of Food Science and Engineering, Guangdong Province Key Laboratory for Green Processing of Natural Products and Product Safety, South China University of Technology, Guangzhou 510640, China*

Xiaoquan Yang − *Laboratory of Food Proteins and Colloids, School of Food Science and Engineering, Guangdong Province Key Laboratory for Green Processing of Natural Products and Product Safety, South China University of Technology, Guangzhou 510640, China*

Complete contact information is available at: https://pubs.acs.org/10.1021/acsami.3c10407

Author Contributions

Q.L.: methodology, investigation, data curation, formal analysis, writing-original draft preparation. X.Y., S.Z., M.X., and Y.Y.: investigation, data curation, formal analysis. Z.W.: methodology, resources, conceptualization, formal analysis, supervision, project administration, writing-review and editing, funding acquisition, validation. X.Y.: project administration, resources, supervision.

Notes

The authors declare no competing financial interest.

■ ACKNOWLEDGMENTS

This work is financially supported by the National Natural Science Foundation of China (Grant 32172347), the Natural Science Foundation of Guangdong Province (Grant

2021A1515011000), the Guangzhou Science and Technology Plan Project (Grant 202201010209), and the 111 Project (Grant B17018).

REFERENCES

(1) Cheng, J.; Amin, D.; Latona, J.; Heber-Katz, E.; Messersmith, P. B. Supramolecular Polymer Hydrogels for Drug-Induced Tissue Regeneration. *ACS Nano* **2019**, *13* (5), 5493−5501.
(2) Draper, E. R.; Adams, D. J. Low-Molecular-Weight Gels: The State of the Art. *Chem* **2017**, *3* (3), 390−410.
(3) Xian, S.; Webber, M. J. Temperature-responsive Supramolecular Hydrogels. *J. Mater. Chem. B* **2020**, *8* (40), 9197−9211.
(4) Hu, B.; Owh, C.; Chee, P. L.; Leow, W. R.; Liu, X.; Wu, Y. L.; Guo, P.; Loh, X. J.; Chen, X. Supramolecular Hydrogels for Antimicrobial Therapy. *Chem. Soc. Rev.* **2018**, *47* (18), 6917−6929.
(5) Dragan, E. S.; Cocarta, A. I. Smart Macroporous IPN Hydrogels Responsive to pH, Temperature, and Ionic Strength: Synthesis, Characterization, and Evaluation of Controlled Release of Drugs. *ACS Appl. Mater. Interfaces* **2016**, *8* (19), 12018−12030.
(6) Mao, L.; Lu, Y.; Cui, M.; Miao, S.; Gao, Y. Design of Gel Structures in Water and Oil Phases for Improved Delivery of Bioactive Food Ingredients. *Crit. Rev. Food Sci. Nutr.* **2020**, *60* (10), 1651−1666.
(7) Bernhard, S.; Tibbitt, M. W. Supramolecular Engineering of Hydrogels for Drug Delivery. *Adv. Drug Delivery Rev.* **2021**, *171*, 240−256.
(8) Song, Z.; Liu, H.; Shen, J.; Chen, X. A Molecular Hydrogel of a Camptothecin Derivative. *Biomater. Sci.* **2013**, *1* (2), 190−193.
(9) Zheng, J.; Fan, R.; Wu, H.; Yao, H.; Yan, Y.; Liu, J.; Ran, L.; Sun, Z.; Yi, L.; Dang, L.; Gan, P.; Zheng, P.; Yang, T.; Zhang, Y.; Tang, T.; Wang, Y. Directed Self-assembly of Herbal Small Molecules into Sustained Release Hydrogels for Treating Neural Inflammation. *Nat. Commun.* **2019**, *10* (1), 1604.
(10) Xu, H.; Wang, T.; Yang, C.; Li, X.; Liu, G.; Yang, Z.; Singh, P. K.; Krishnan, S.; Ding, D. Supramolecular Nanofibers of Curcumin for Highly Amplified Radiosensitization of Colorectal Cancers to Ionizing Radiation. *Adv. Funct. Mater.* **2018**, *28* (14), No. 1707140.
(11) Webber, M. J.; Langer, R. Drug Delivery by Supramolecular Design. *Chem. Soc. Rev.* **2017**, *46* (21), 6600−6620.
(12) Chivers, P. R. A.; Smith, D. K. Shaping and Structuring Supramolecular Gels. *Nat. Rev. Mater.* **2019**, *4* (7), 463−478.
(13) Primo, G. A.; Mata, A. 3D Patterning within Hydrogels for the Recreation of Functional Biological Environments. *Adv. Funct. Mater.* **2021**, *31* (16), No. 2009574.
(14) Li, J.; Mooney, D. J. Designing Hydrogels for Controlled Drug Delivery. *Nat. Rev. Mater.* **2016**, *1* (12), 16071.
(15) Lu, C. H.; Yeh, Y. C. Fabrication of Multiresponsive Magnetic Nanocomposite Double-Network Hydrogels for Controlled Release Applications. *Small* **2021**, *17* (522), No. e2105997.
(16) Zhao, Y.; Chen, S.; Hu, J.; Yu, J.; Feng, G.; Yang, B.; Li, C.; Zhao, N.; Zhu, C.; Xu, J. Microgel-Enhanced Double Network Hydrogel Electrode with High Conductivity and Stability for Intrinsically Stretchable and Flexible All-Gel-State Supercapacitor. *ACS Appl. Mater. Interfaces* **2018**, *10* (23), 19323−19330.
(17) Piras, C. C.; Slavik, P.; Smith, D. K. Self-Assembling Supramolecular Hybrid Hydrogel Beads. *Angew. Chem., Int. Ed. Engl.* **2020**, *59* (2), 853−859.
(18) Eelkema, R.; Pich, A. Pros and Cons: Supramolecular or Macromolecular: What is Best for Functional Hydrogels with Advanced Properties? *Adv. Mater.* **2020**, *32* (20), No. e1906012.
(19) Cornwell, D. J.; Smith, D. K. Expanding the Scope of Gels-combining Polymers with Low-Molecular-Weight Gelators to Yield Modified Self-assembling Smart Materials with High-tech Applications. *Mater. Horiz.* **2015**, *2* (3), 279−293.
(20) Cornwell, D. J.; Okesola, B. O.; Smith, D. K. Hybrid Polymer and Low Molecular Weight Gels-Dynamic Two-component Soft Materials with Both Responsive and Robust Nanoscale Networks. *Soft Matter* **2013**, *9* (36), 8730.
(21) Su, X.; Wu, L.; Hu, M.; Dong, W.; Xu, M.; Zhang, P. Glycyrrhizic acid: A Promising Carrier Material for Anticancer Therapy. *Biomed. Pharmacother.* **2017**, *95*, 670−678.
(22) Zhao, Z.; Xiao, Y.; Xu, L.; Liu, Y.; Jiang, G.; Wang, W.; Li, B.; Zhu, T.; Tan, Q.; Tang, L.; Zhou, H.; Huang, X.; Shan, H. Glycyrrhizic Acid Nanoparticles as Antiviral and Anti-inflammatory Agents for COVID-19 Treatment. *ACS Appl. Mater. Interfaces* **2021**, *13* (18), 20995−21006.
(23) Yu, S.; Zhu, Y.; Xu, J.; Yao, G.; Zhang, P.; Wang, M.; Zhao, Y.; Lin, G.; Chen, H.; Chen, L.; Zhang, J. Glycyrrhizic Acid Exerts Inhibitory Activity Against the Spike Protein of SARS-CoV-2. *Phytomedicine* **2021**, *85*, No. 153364.
(24) Tian, J.; Li, X.; Zhao, L.; Shen, P.; Wang, Z.; Zhu, L.; Li, C.; Su, C.; Zhang, Y. Glycyrrhizic Acid Promotes Neural Repair by Directly Driving Functional Remyelination. *Food Funct.* **2020**, *11* (1), 992−1005.
(25) Saha, A.; Adamcik, J.; Bolisetty, S.; Handschin, S.; Mezzenga, R. Fibrillar Networks of Glycyrrhizic Acid for Hybrid Nanomaterials with Catalytic Features. *Angew. Chem., Int. Ed. Engl.* **2015**, *54* (18), 5408−5412.
(26) Wan, Z.; Sun, Y.; Ma, L.; Guo, J.; Wang, J.; Yin, S.; Yang, X. Thermoresponsive Structured Emulsions Based on the Fibrillar Self-assembly of Natural Saponin Glycyrrhizic Acid. *Food Funct.* **2017**, *8* (1), 75−85.
(27) Wu, J.; Yu, X.; Zhang, H.; Guo, J.; Hu, J.; Li, M.-H. Fully Biobased Vitrimers from Glycyrrhizic Acid and Soybean Oil for Self-Healing, Shape Memory, Weldable, and Recyclable Materials. *ACS Sustainable Chem. Eng.* **2020**, *8* (16), 6479−6487.
(28) Ma, Y.; Hao, J.; Zhao, K.; Ju, Y.; Hu, J.; Gao, Y.; Du, F. Biobased Polymeric Surfactant: Natural Glycyrrhizic Acid-appended Homopolymer with Multiple pH-responsiveness. *J. Colloid Interface Sci.* **2019**, *541*, 93−100.
(29) Li, Q.; Wan, Z.; Yang, X. Glycyrrhizic acid: Self-assembly and Applications in Multiphase Food Systems. *Curr. Opin. Food Sci.* **2022**, *43*, 107−113.
(30) Su, E.; Li, Q.; Xu, M.; Yuan, Y.; Wan, Z.; Yang, X.; Binks, B. P. Highly Stable and Thermo-responsive Gel Foams by Synergistically Combining Glycyrrhizic Acid Nanofibrils and Cellulose Nanocrystals. *J. Colloid Interface Sci.* **2021**, *587*, 797−809.
(31) Ma, L.; Bertsch, P.; Wan, Z.; Yang, X.; Fischer, P. Synergistic Effect of Glycyrrhizic Acid and Cellulose Nanocrystals for Oil-Water Interfacial Stabilization. *Food Hydrocolloids* **2021**, *120*, No. 106888.
(32) Li, Q.; Xu, M.; Xie, J.; Su, E.; Wan, Z.; Sagis, L. M. C.; Yang, X. Large Amplitude Oscillatory Shear (LAOS) for Nonlinear Rheological Behavior of Heterogeneous Emulsion Gels Made from Natural Supramolecular Gelators. *Food Res. Int.* **2021**, *140*, No. 110076.
(33) Li, Q.; Zhang, S.; Du, R.; Yang, Y.; Liu, Y.; Wan, Z.; Yang, X. Injectable Self-Healing Adhesive Natural Glycyrrhizic Acid Bioactive Hydrogel for Bacteria-Infected Wound Healing. *ACS Appl. Mater. Interfaces* **2023**, *15* (14), 17562−17576.
(34) Tang, S.; Yang, J.; Lin, L.; Peng, K.; Chen, Y.; Jin, S.; Yao, W. Construction of Physically Crosslinked Chitosan/Sodium Alginate/Calcium Ion Double-Network Hydrogel and Its Application to Heavy Metal Ions Removal. *Chem. Eng. J.* **2020**, *393*, No. 124728.
(35) Yu, F.; Cui, T.; Yang, C.; Dai, X.; Ma, J. Kappa-Carrageenan/Sodium Alginate Double-Network Hydrogel with Enhanced Mechanical Properties, Anti-Swelling, and Adsorption Capacity. *Chemosphere* **2019**, *237*, No. 124417.
(36) Yang, Y.; Chen, X.; Li, Y.; Yin, Z.; Bao, M. Construction of a Superhydrophobic Sodium Alginate Aerogel for Efficient Oil Absorption and Emulsion Separation. *Langmuir* **2021**, *37* (2), 882−893.
(37) Hyun, K.; Wilhelm, M.; Klein, C. O.; Cho, K. S.; Nam, J. G.; Ahn, K. H.; Lee, S. J.; Ewoldt, R. H.; McKinley, G. H. A Review of Nonlinear Oscillatory Shear Tests: Analysis and Application of Large Amplitude Oscillatory Shear (LAOS). *Prog. Polym. Sci.* **2011**, *36* (12), 1697−1753.

https://doi.org/10.1021/acsami.3c10407
ACS Appl. Mater. Interfaces 2023, 15, 43633−43647

(38) Lu, S.; Yang, Y.; Yao, J.; Shao, Z.; Chen, X. Exploration of the Nature of a Unique Natural Polymer-based Thermosensitive Hydrogel. *Soft Matter* **2016**, *12* (2), 492−499.
(39) Ewoldt, R. H.; Hosoi, A. E.; McKinley, G. H. New Measures for Characterizing Nonlinear Viscoelasticity in Large Amplitude Oscillatory Shear. *J. Rheol.* **2008**, *52* (6), 1427−1458.
(40) Duvarci, O. C.; Yazar, G.; Kokini, J. L. The Comparison of LAOS Behavior of Structured Food Materials (Suspensions, Emulsions, and Elastic Networks). *Trends Food Sci. Technol.* **2017**, *60*, 2−11.
(41) Tarashi, S.; Nazockdast, H.; Bandegi, A.; Shafaghsorkh, S.; Sodeifian, G.; Foudazi, R. Large Amplitude Oscillatory Shear Behavior of Thermoresponsive Hydrogels: Single Versus Double Network. *J. Rheol.* **2023**, *67* (1), 15−33.
(42) Anvari, M.; Tabarsa, M.; Joyner, H. S. Large Amplitude Oscillatory Shear Behavior and Tribological Properties of Gum Extracted from Alyssum Homolocarpum Seed. *Food Hydrocolloids* **2018**, *77*, 669−676.
(43) Ramya, K. A.; Reddy, S. M. M.; Shanmugam, G.; Deshpande, A. P. Fibrillar Network Dynamics during Oscillatory Rheology of Supramolecular Gels. *Langmuir* **2020**, *36* (44), 13342−13355.
(44) Onck, P. R.; Koeman, T.; van Dillen, T.; van der Giessen, E. Alternative Explanation of Stiffening in Cross-Linked Semiflexible Networks. *Phys. Rev. Lett.* **2005**, *95* (17), No. 178102.
(45) Cook, M. T.; Tzortzis, G.; Charalampopoulos, D.; Khutoryanskiy, V. V. Production and Evaluation of Dry Alginate-Chitosan Microcapsules as An Enteric Delivery Vehicle for Probiotic Bacteria. *Biomacromolecules* **2011**, *12* (7), 2834−2840.
(46) Kang, H.; Wen, Q.; Janmey, P. A.; Tang, J. X.; Conti, E.; MacKintosh, F. C. Nonlinear Elasticity of Stiff Filament Networks Strain Stiffening, Negative Normal Stress, and Filament Alignment in Fibrin Gels. *J. Phys. Chem. B* **2009**, *113*, 3799−3805.
(47) Ewoldt, R. H.; Winter, P.; Maxey, J.; McKinley, G. H. Large Amplitude Oscillatory Shear of Pseudoplastic and Elastoviscoplastic Materials. *Rheol. Acta* **2010**, *49* (2), 191−212.
(48) Cadix, A.; Chassenieux, C.; Lafuma, F. O.; Lequeux, F. O. Control of the Reversible Shear-induced Gelation of Amphiphilic Polymers through Their Chemical Structure. *Macromolecules* **2005**, *38*, 527−536.

https://doi.org/10.1021/acsami.3c10407
ACS Appl. Mater. Interfaces 2023, 15, 43633−43647